Contribution from the Department of Chemistry,
McMaster University, Hamilton, Ontario, Canada L8S 4M1

Molecular Geometry and Fluxionality in the AX_6E System ClF_6^-

Preston J. MacDougall

Received June 20, 1985

Gillespie's VSEPR model predicts AX_6E systems to be distorted from octahedral symmetry. This paper tests, and strengthens, the suggestion that AX_6E systems should distort from O_h symmetry in the gaseous state because of the presence of a stereochemically active lone pair. This is done by examining the Laplacian of the calculated electronic charge distribution of ClF_6^-. It has been shown that this function assimilates Lewis' concept of electron pairs. Bartell and Gavin have qualitatively invoked the second-order Jahn-Teller model (SOJT) to rationalize the fluxionality of XeF_6. This model is briefly reviewed and applied to ClF_6^- to further examine the importance of the SOJT effect in AX_6E systems. The connection between the static properties, successfully described by the charge distribution, and the dynamical properties, qualitatively predicted by the SOJT model, is discussed.

Introduction

The molecular geometry of XeF_6 is predicted, by using Gillespie's VSEPR model, to be a distorted octahedron with C_{3v} symmetry, i.e., an "octahedron" with one face expanded and the opposite face contracted. XeF_6 is an AX_6E system (the central atom is hexacoordinated with one unshared pair of electrons); thus, the VSEPR model attributes its distorted geometry to the presence of a "lone pair" in the expanded face.[1] Bartell and Gavin have concluded from electron diffraction data that XeF_6, in the gas phase, is not a regular octahedron and that the distribution of the diffraction peaks suggested rapidly interconverting non-O_h geometries (via a facile t_{1u} bending mode).[2] Burbank and Jones have reported X-ray crystallographic results for XeF_6 in the solid state that verify a distorted octahedral geometry around the xenon atom.[3] However, polymers formed by F bridging make up the unit cell; therefore, the non-octahedral geometry is not simply the result of a stereochemically active lone pair. Weighting heavily against the VSEPR model are the vast majority of crystal structures containing ions isoelectronic with XeF_6, such as $TeCl_6^{2-}$, $TeBr_6^{2-}$, and $SbBr_6^{3-}$.[4] In nearly every case the geometry around the central atom is that of a regular octahedron. In this class of molecules the VSEPR model appears to rationalize the exception rather than the rule. Infrared and Raman studies of some of the ions in solution also support octahedral geometries.[5]

Recently, Bader et al. have shown that the Laplacian of the electronic charge distribution, the function $\nabla^2\rho(\mathbf{r})$, can be used to test the tenets of the VSEPR model.[6] The function $\nabla^2\rho$ maps out regions of *local* charge concentration, $\nabla^2\rho < 0$, and regions of *local* charge depletion, $\nabla^2\rho > 0$. For charge to be *locally* concentrated at a position $\mathbf{r}$ the value of ρ need only be greater than the *average* of the values of ρ at all neighboring points. Maxima in local charge concentration (maxima in $-\nabla^2\rho$) have been shown to correlate well with Lewis' idea of bonded and nonbonded electron pairs.[7] Since $\nabla^2\rho$ is a property of the total charge density, neither an orthonormal transformation of the canonical molecular orbitals to an equivalent (localized) set[8] nor subtraction of superimposed densities of atoms in arbitrary reference states[9] are necessary to recover the above connection with valence-bond models.

The Laplacian distribution has also been shown to provide a general classification of atomic interactions.[10] It is observed that there are two limiting types of atomic interactions as defined by the properties of $\rho(r)$, closed-shell and shared interactions. The Laplacian distribution also recovers the shell model of an atom by displaying a spherical shell of local charge concentration enveloped by a spherical shell of local charge depletion for each quantum shell of an atom.[10] These properties of the Laplacian distribution will be discussed in detail in the next section.

The ClF_6^- ion is an AX_6E system that has not yet been observed.[11] This paper presents an analysis of the calculated charge distributions and corresponding Laplacian distributions of this ion in both its equilibrium geometry (C_{3v}) and its fluxional transition state geometry (C_{2v}). A corresponding analysis of ClF_3, which is not fluxional, is presented for contrast.

The large amplitude of the t_{1u} displacements in XeF_6 has been rationalized by Bartell and Gavin using the second-order Jahn-Teller (SOJT) model for predicting facile modes of vibration.[12] With the SOJT model, the vibrational behavior of ClF_6^- is predicted to be analogous to that observed for XeF_6. A possible explanation of the previously mentioned VSEPR exceptions, based on the properties of their charge distributions, is also presented.

Properties of the Laplacian Distribution

The locations of maxima, minima, or saddle points in a scalar function such as the charge density or its Laplacian are determined by the positions of critical points in these functions, points where either $\nabla\rho = 0$ or $\nabla(\nabla^2\rho) = 0$. Whether the function is a maximum, minimum, or saddle at a given critical point is determined by the curvatures of the function at that point.[13] Since charge is locally concentrated where $\nabla^2\rho < 0$, it is more convenient to work with the function $-\nabla^2\rho$, a maximum in this function being a maximum in local charge concentration.

The valence shell of charge concentration (VSCC) of an isolated atom possesses a spherical surface over which the charge is maximally concentrated; i.e., $\nabla(\nabla^2\rho) = 0$ for every point on the surface. Thus the curvature of $-\nabla^2\rho$ normal to this surface, the radial curvature, is negative. The two remaining curvatures, those tangential to the surface, are equal to zero. In general this surface persists when the atom is in chemical combination (the derivative of $-\nabla^2\rho$ normal to the surface is still zero and the corresponding curvature is negative), but the surface is no longer one of uniform concentration as the tangential curvatures assume either positive or negative values. If a local maximum is formed on the surface, then the two tangential curvatures of $-\nabla^2\rho$ are negative. For example, the VSCC of the Cl atom in ClF_3 exhibits five maxima

(1) Gillespie, R. J. *Angew. Chem., Int. Ed. Engl.* **1967**, *6*, 819.
(2) Bartell, L. S.; Gavin, R. M., Jr. *J. Chem. Phys.* **1968**, *48*, 2466.
(3) Burbank, R. D.; Jones, G. R. *J. Am. Chem. Soc.* **1974**, *96*, 43.
(4) Engel, G. *Z. Kristallogr., Kristallgeom., Kristalphys., Kristallchem.* **1935**, *90*, 341. Aynsley, E. E.; Hazell, A. C. *Chem. Ind. (London)* **1963**, 611. Brown, I. D. *Can. J. Chem.* **1964**, *42*, 2758.
(5) Beattie, I. R.; Chudzynska, H. *J. Chem. Soc.* **1967**, 984. Spragg, R. A.; Stammereich, H.; Kawano, Y. *J. Mol. Struct.* **1969**, *3*, 305.
(6) Bader, R. F. W.; MacDougall, P. J.; Lau, C. D. H. *J. Am. Chem. Soc.* **1984**, *106*, 1594.
(7) Lewis, G. N. *J. Am. Chem. Soc.* **1916**, *33*, 762.
(8) Lennard-Jones, J. E. *Proc. R. Soc. London, A* **1949**, *198*, I, 14.
(9) Roux, M.; Besnainou, S.; Daudel, R. *J. Chim. Phys. Phys.-Chim. Biol.* **1956**, *54*, 218.
(10) Bader, R. F. W.; Essén, H. *J. Chem. Phys.* **1984**, *80*, 1943.
(11) The preparation of ClF_6^- has been reported in a U.S. patent, but details of its characterization have not been published: Faust, J. P.; Jacke, A. W.; Klanica, A. J. *Chem. Abstr.* **1973**, *79*, 55557y.
(12) Bader, R. F. W. *Mol. Phys.* **1960**, *3*, 137. Bader, R. F. W. *Can. J. Chem.* **1962**, *40*, 1164.
(13) If all three curvatures are negative at a critical point, the function is at a maximum; if all three are positive, it is at a minimum. Saddle points are obtained when the critical point is viewed in a plane and one curvature is negative and the other positive. The third curvature in these cases may be of either sign.

0020-1669/86/1325-4400$01.50/0

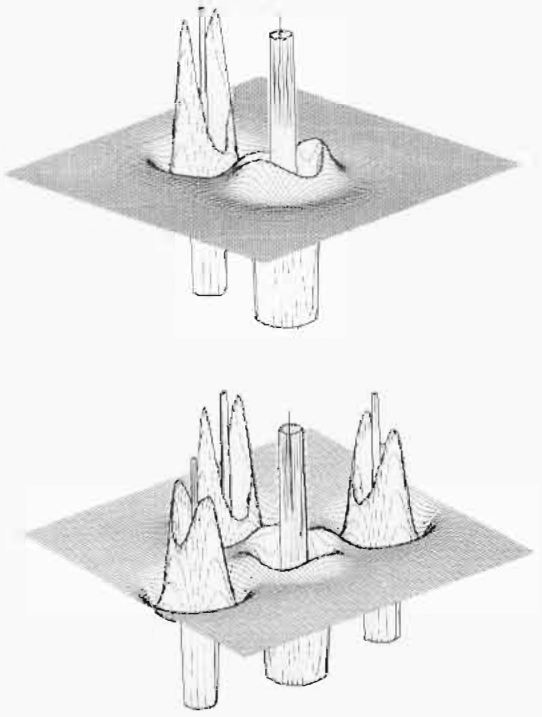

Figure 1. Relief maps of $-\nabla^2\rho$ for the equatorial (upper) and axial (lower) planes in ClF_3. Note the presence of three quantum shells centered on the Cl atom as opposed to only two on the F atoms. Since an F^- ion exhibits a spherical VSCC, it can be seen from this diagram that the axial F's are more like F^- than the equatorial ones.

in $-\nabla^2\rho$, three bonded and two nonbonded maxima (Figure 1).[3]

The Laplacian distribution also provides a means of classifying atomic interactions. Two atoms are said to interact directly only when they share an interatomic surface as defined within Bader et al.'s quantum theory of atoms in molecules.[14] Bader has recently reviewed this theory for the general reader.[15] If two atoms share an interatomic surface there necessarily exists a line linking the two nuclei along which the charge density is a maximum with respect to perpendicular displacement. This is called an *atomic interaction line*. The point at which ρ reaches its minimum value along the atomic interaction line is denoted $\mathbf{r}_c$; this is the point of intersection of the interatomic surface and the atomic interaction line. In a bound system an atomic interaction line is called a *bond path*.[10,15] The value of $\nabla^2\rho(\mathbf{r}_c)$ is the sum of the three orthogonal curvatures of ρ at r_c, the positive one is parallel to the atomic interaction line and the two negative curvatures are perpendicular to it. Thus if $\nabla^2\rho(\mathbf{r}_c) \ll 0$ the perpendicular curvatures dominate the parallel curvature. This corresponds to ρ starting off at a large value at $\mathbf{r}_c$ and falling off rapidly in all directions perpendicular to the atomic interaction line. At the other extreme, if $\nabla^2\rho(\mathbf{r}_c) \gg 0$, the parallel curvature dominates the perpendicular curvatures. This corresponds to $\rho(r)$ being relatively flat in the interatomic surface (i.e., $\rho(\mathbf{r}_c)$ is small and decreases slowly in all perpendicular directions) while increasing rapidly toward each nucleus.

Bader and Essén have observed the following characteristics for the two limiting types of atomic interactions: (a) Shared interactions, such as N_2 (Figure 2), exhibit large values of $\rho(\mathbf{r}_c)$ and negative values of $\nabla^2\rho(\mathbf{r}_c)$. (b) Closed-shell interactions, such as Ar_2 (Figure 2), exhibit small values of $\rho(\mathbf{r}_c)$ and positive values of $\nabla^2\rho(\mathbf{r}_c)$.[10] It is of particular significance to this work that not only do noble-gas repulsive states and ionic systems belong to the class of closed-shell interactions, but interactions between atoms that possess a high degree of electron localization also belong to this class.[10,16] The degree of localization of electrons on atom

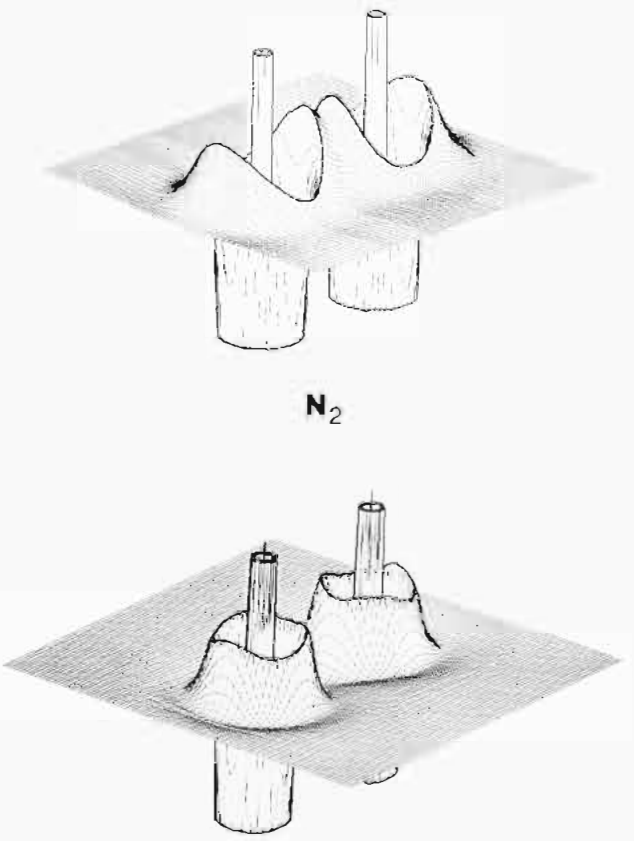

Figure 2. Relief maps of $-\nabla^2\rho$ for planes containing the nuclei for N_2 and Ar_2 (R = 4.0 au). In N_2 the VSCC's of the N atoms are joined together and charge is locally concentrated in the interatomic surface, while in Ar_2 the VSCC's are separately localized on each Ar atom and charge is locally depleted in the interatomic surface.

Ω is defined as $I(\Omega) = |F(\Omega,\Omega)/N(\Omega)|$, where $F(\Omega,\Omega)$ is obtained by integrating the Fermi hole over the atom Ω and $N(\Omega)$ is the average electron population of atom Ω.[17] Complete localization corresponds to no *inter*atomic exchange of the electrons on atom Ω, a situation achieved only by isolated atoms. However, very electronegative atoms exhibit large degrees of localization even in molecules conventionally described as covalent or shared interactions, such is the case in F_2 [I(F) = 93%].[10]

Another characteristic of closed-shell interactions is that they possess little directional character, resulting in very floppy bonds. The C–Li bonds in triplet CLi_2 are ionic [q(Li) = +0.912e]; hence, they exhibit a closed-shell atomic interaction [$\rho(\mathbf{r}_c)$ = 0.035 au and $\nabla^2\rho(\mathbf{r}_c)$ = +0.224 au]. The energy difference between the linear and equilibrium geometries (θ = 111.9°) is only 1.4 kcal/mol.[18]

The SOJT Model

The second-order Jahn–Teller model treats nuclear displacements as perturbations and uses perturbation theory to determine what effect these displacements have on the electronic energy of the molecule in question.[12] For displacement from an equilibrium geometry in the mode Q_i the correction to the electronic energy, correct to second order, is given by

$$\Delta E(Q_i) = \tfrac{1}{2}[V_{00}^{ii} + 2\sum_k{}' |V_{0k}^i|^2/(E_0 - E_k)]\delta Q_i^2 \qquad (1)$$

The first term is the contribution to ΔE arising from the nuclear

(14) Bader, R. F. W.; Nguyen-Dang, T. T.; Tal, Y. *J. Chem. Phys.* **1979**, *70*, 4316. Bader, R. F. W.; Nguyen-Dang, T. T.; Tal, Y. *Rep. Prog. Phys.* **1981**, *44*, 893.
(15) Bader, R. F. W. *Acc. Chem. Res.* **1985**, *18*, 9.
(16) Tang, T.-H.; Bader, R. F. W.; MacDougall, P. J. *Inorg. Chem.* **1985**, *24*, 2047.
(17) Bader, R. F. W.; Stephens, M. E. *J. Am. Chem. Soc.* **1975**, *97*, 7391.
(18) MacDougall, P. J.; Bader, R. F. W. *Can. J. Chem.* **1985**, *64*, 1496.

Table I. Geometries and Energies of ClF_3 and ClF_6^- Systems

system	geometry	geometrical parameters[a] dist, Å; angles, deg	energy, hartrees	ΔE,[b] kcal/mol
ClF_3	optimized T-shape	$Cl-F_{ax}$ = 1.682, $Cl-F_{eq}$ = 1.607; $\angle F_{ax}ClF_{eq}$ = 85.36	−757.03423	
ClF_3	planar fluxional transition state	$Cl-F_{eq}$ = 1.709; ∠FClF = 120.0	−756.96134	+45.7
ClF_6^- (Figure 4)	optimized C_{3v} distorted octahedron	Cl–F1 = 1.859, Cl–F4 = 1.627; ∠nClF1 = 67.04, ∠nClF4 = 127.51	−1054.67174	
ClF_6^- (Figure 4)	C_{2v} fluxional transition state	Cl–F2 = 1.910, Cl–F1 = 1.701, Cl–F5 = 1.625; ∠nClF2 = 57.37, ∠nClF1 = 96.54, ∠nClF5 = 138.30	−1054.66978	+1.23

[a] n refers to the location of the nonbonded charge concentration, in the C_{3v} structure this is in the center of the F1F2F3 face while in the C_{2v} structure it is in the center of the F2F3 edge. [b] $\Delta E = E$(transition-state geometry) − E(optimized geometry).

displacement in the presence of the *undisturbed* charge density ρ_{00}. The final term represents the contribution to ΔE arising from the *change* in ρ caused by the nuclear displacement

$$V^i_{0k} = \int (\partial V_{ne}/\partial Q_i)\rho_{0k}\, d\tau \qquad (2)$$

The transition density, ρ_{0k}, is the change in ρ_{00} following "mixing-in" with the ground-state function, ψ_0, the singly excited state function, ψ_k.[12]

The only change in ρ_{00} that causes a change in the electronic energy is that which does not correspond to rigid following of the nuclei. This change is called the *relaxation* in ρ_{00}.[12] From eq 2 the integral V^i_{0k} vanishes unless ρ_{0k} and Q_i have identical symmetries. Given the above constraints and the fact that $(E_0 - E_k)$ appears in the denominator of the second term in eq 2, Bader approximates the relaxation in ρ_{00} for any mode Q_i as a single ρ_{0k}, that arising from "mixing-in" the lowest excited state of appropriate symmetry.[12] In this work, and other recent work,[19] ρ_{0k} is approximated as a product of the HOMO and LUMO of a single determinantal wave function, ψ_0.

The SOJT model predicts that the symmetry of the molecular vibration with the lowest force constant will be the same as the symmetry of the transition density corresponding to HOMO → LUMO excitation.[12] In simple terms, the force constant is low because the electron density can easily relax in such a way that the increase in energy, during motion away from the equilibrium geometry in this mode, is minimized.

Calculations

Ab initio calculations made by using Gaussian 80 were performed for ClF_3 and ClF_6^-.[20] The equilibrium and fluxional transition-state geometries for ClF_3 and ClF_6^- were separately optimized with the 6-21G* basis set. The energies and geometrical parameters are reported in Table I. The symmetries of the fluxional transition states were chosen by using the SOJT model. Other calculations have shown that the equilibrium geometry of XeF_6 has C_{3v} symmetry.[21] Atomic and bond properties were calculated from the ab initio wave functions by using the PROAIM package.[22]

Fluxionality of ClF_6^- in Terms of the SOJT Model

The calculated equilibrium geometry of ClF_6^- is a distorted octahedron (C_{3v}), as predicted by the VSEPR model. The symmetries of HOMO and LUMO in ClF_6^- are a_1 and e, respectively (the degenerate LUMO's and the next lowest virtual orbital, a_1, correlate with the t^*_{1u} orbitals in the O_h point group). Therefore the symmetry of the easiest mode of vibration is E (this bend correlates with the T_{1u} bend in O_h symmetry). The transition density accompanying this mode is illustrated in Figure 3 (please refer to Figure 4 for the numbering scheme). There are two degenerate ρ_{0k}'s; the one symmetric with respect to reflection in a σ_v plane of symmetry is shown for clarity. The directions of the arrows in Figure 3 indicate the approximate motion of the nuclei that is enhanced by this transition density. As can be seen by comparing the molecular graphs (the network of bond paths[14]) in Figure 4 or the geometrical parameters in Table I, the motion of each nucleus as predicted by the SOJT model is that which takes the molecule from the C_{3v} geometry to the C_{2v} transition state. The transition state is only 1.2 kcal/mol less stable than the equilibrium geometry; hence, this molecule should be very fluxional. The SOJT model attributes this low barrier partly to the low HOMO–LUMO energy difference (0.48 au), when compared to the corresponding value for ClF_3 (0.59 au), which is not fluxional. Others have observed that the HOMO–LUMO energy difference decreases for increasing fluorination in XeF_n

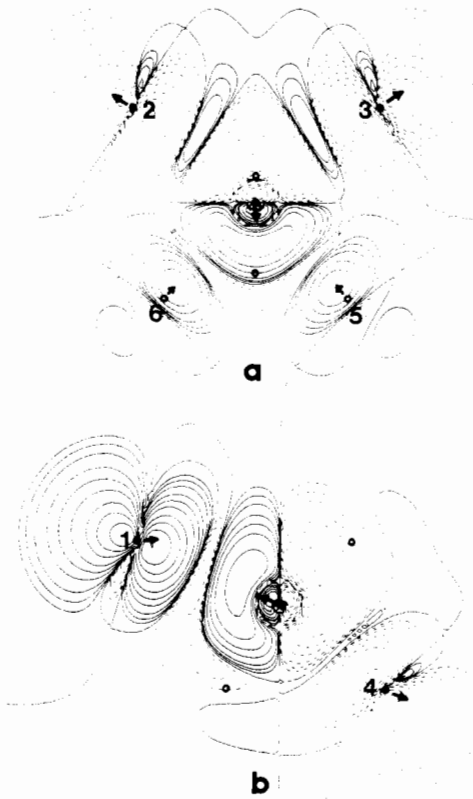

Figure 3. Contour maps of the transition density corresponding to HOMO → LUMO excitation for ClF_6^-. The lower diagram is of a plane of symmetry containing F1, Cl, and F4 (see Figure 4 for numbering scheme). The upper diagram is of a plane containing Cl and a long edge of the distorted octahedron (F2, F3 in this case). The arrows indicate the directions of the nuclear motions if charge is removed from regions denoted by dashed contours and accumulated in regions denoted by solid contours. The values of the contours are ±0.0002, ±0.0004, and ±0.0008 increasing in powers of 10 to ±8.0. Positions of in-plane nuclei are denoted by solid circles; the projected positions of out-of-plane nuclei are denoted by open circles (F5 and F6 are only slightly out of this plane, thus the direction of their motion can be inferred from this plot).

(19) Bader, R. F. W.; MacDougall, P. J. *J. Am. Chem. Soc.* **1985**, *107*, 6788.
(20) Binkley, J. S.; Whiteside, R. A.; Krishnan, R.; Seeger, R.; DeFrees, D. J.; Schlegel, H. B.; Topiol, S.; Kahn, L. R.; Pople, J. A. Carnegie-Mellon University.
(21) Rothman, M. J.; Bartell, L. S.; Ewig, C. S.; Van Wazer, J. R. *J. Chem. Phys.* **1980**, *73*, 375.
(22) Biegler-König, F. W.; Bader, R. F. W.; Tang, T.-H. *J. Comput. Chem.* **1982**, *13*, 317.

Table II. Atomic Properties of ClF_3 and ClF_6^- Systems

system	atomic properties			bond properties		
	atom	$q(\Omega)$[a]	l(F), %	bond	ρ_b,[b] au	$\nabla^2\rho_b$,[b] au
ClF_3 (T-shaped)	Cl	+1.34		$Cl-F_{ax}$	0.195	−0.057
	F_{ax}	−0.52	94.3	$Cl-F_{eq}$	0.237	−0.241
	F_{eq}	−0.30	93.3			
ClF_3 (planar)	Cl	+1.46		Cl−F	0.182	+0.153
	F	−0.49	94.0			
ClF_6^- (C_{3v})	Cl	+3.20		Cl−F1	0.139	+0.255
	F1(2,3)	−0.66	95.5	Cl−F4	0.235	−0.180
	F4(5,6)	−0.41	93.5			
ClF_6^- (C_{2v})	Cl	+3.20		Cl−F2	0.125	+0.258
	F2(3)	−0.70	95.9	Cl−F1	0.198	+0.071
	F1(4)	−0.50	94.3	Cl−F5	0.238	−0.196
	F5(6)	−0.40	93.4			

[a] $q(\Omega)$ is the net charge on Ω, $q(\Omega) = Z(\Omega) - \int_\Omega \rho\, d\tau$. [b] ρ_b and $\nabla^2\rho_b$ are defined as the respective values of $\rho(\mathbf{r})$ and $\nabla^2\rho(\mathbf{r})$ at the bond, or the (3, −1), critical point.

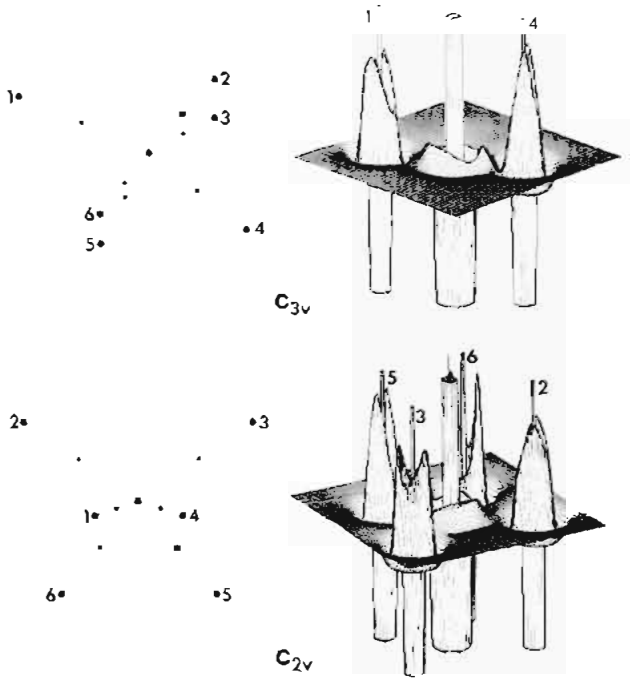

Figure 4. Left: molecular graphs (projections of the bond paths) for the C_{3v} and C_{2v} geometries of ClF_6^-. In the lower molecular graph the Cl−F1(4) bond paths are coming out of (going into) the projection plane. The large dots denote the projected positions of the nuclei. The small dots denote the projected positions of the bond critical points. Right: relief maps of $-\nabla^2\rho$. As in Figure 1 the more spherical VSCC's of the F atoms nearest the nonbonded charge concentration on Cl indicate the bonds to these atoms are more closed shell in nature. Note that the VSCC of the Cl atom does not exhibit maxima along the long Cl−F bonds in either geometry, only shoulders at the edge of the nonbonded maxima.

systems.[21] The symmetries of HOMO and LUMO in ClF_3 are both a_1; hence, the nuclear motion enhaced by the SOJT effect is of A_1 symmetry [$\nu_3(A_1)$ for C_{2v} AZX_2 systems]. The resulting motion of the nuclei leads to the D_{3h} geometry (Table I), which is a pseudorotation transition state since all F's are equivalent. The energy barrier to this pseudorotation (45.7 kcal/mol) is much greater than that for ClF_6^-.

Geometry and Fluxionality in Terms of Atomic Properties

The molecular graph of ClF_6^- in its equilibrium geometry (Figure 4) illustrates the marked effect that the nonbonded electrons on Cl have on the molecular geometry. The valence shell of charge concentration, VSCC, of the Cl atom exhibits a nonbonded maximum in $-\nabla^2\rho$ in both the C_{3v} and C_{2v} geometries. This is characteristic of atoms possessing unshared electrons.[6] Figure 4 shows that in the C_{3v} geometry the nonbonded maximum is located in the widened triangular face (F1F2F3). In accord with the VSEPR model[1] the bonded maxima on Cl most removed from the position of the nonbonded maximum are the largest in size and extent of local charge concentration, such as the maxima along the Cl−F4 bond in Figure 4.[23] This behaviour can also be seen in ClF_3 (Figure 1), although the difference between the equatorial bonded maximum and the two axial bonded maxima is less pronounced as a result of the smaller extent to which their positions relative to the nonbonded maxima differ. Figure 4 shows that in the C_{2v} transition state the nonbonded maxima is "squeezed" between the Cl−F2 and Cl−F3 bonds and is less pronounced as a maximum in the VSCC.

The properties of the atoms in ClF_6^-, and ClF_3 for comparison, are listed in Table II. There is a clear trend for the F atoms nearest the nonbonded maxima (maximum) to be the most negatively charged and to exhibit the largest degree of localization. The VSEPR model predicts that these F's will have the largest Cl−F distances because of lone-pair–bond-pair repulsions.[24] Thus it is seen here that where VSEPR predicts longer bonds resulting from pair repulsions, a larger degree of ionicity of the bond in question also results. This greater ionicity is reflected in the atomic interactions as a more closed-shell interaction between Cl and the F's nearest the nonbonded maxima (maximum), i.e., lower ρ_b and more positive $\nabla^2\rho_b$ values (Table II). The data in Table II also reveal that the fluxional transition states have greater atomic localization and more closed-shell type interactions than the equilibrium geometries, when averaged over the molecule. In ClF_3 the $Cl-F_{eq}$ bond undergoes a much greater increase in ionicity and atomic localization during the process of pseudorotation than any of the bonds in ClF_6^-. This suggests that the greater the reorganization of the charge distribution necessary for pseudorotation (reflected by the properties of the atoms), the more difficult pseudorotation will be. The extreme closed-shell nature of the Cl−F2(3) bonds in the transition state of ClF_6^- indicates that only electrostatic attraction holds this molecule together as it undergoes its rapid $C_{3v} \rightarrow C_{2v} \rightarrow C_{3v}$ interconversion. This is thought to be the case for XeF_6 as well.[25]

The octahedral geometries of $TeCl_6^{2-}$ and other VSEPR exceptions[4,5] in the condensed phases may be a result of the nonbonded charge concentration on the central atom not exerting a strong enough force on the neighboring bonded charge concentrations to distort the molecule. This would be the case if the atomic interactions in these systems were more ionic in nature

(23) In fact the three bonded charge concentrations along the long Cl−F bonds are so poorly defined, as a result of the closed-shell nature of the atomic interactions, that they do not form maxima but only three shoulders on the edge of the nonbonded maximum on Cl. The same is true to a greater extent for the even longer Cl−F2(3) bonds in the transition state. The C atom in triplet CCl_2 (which has ionic bonds) behaves similarly; i.e., it does not possess bonded maxima in its VSCC, only nonbonded maxima.[15]

(24) Gillespie, R. J. *Molecular Geometry*; Van Nostrand Rheinhold: London, 1972.

(25) Schrobilgen, G. J., personal communication. Hyman, H. H.; Quarterman, L. A. *Noble-Gas Compounds*; Hyman, H. H., Ed.; University Chicago Press: Chicago, 1963.

than those in XeF_6 and ClF_6^-, resulting in minimal concentration of charge on the *central* atom along the bond paths, i.e., very small, if any, bonded maxima for the nonbonded maximum to repel. In ref 6 the effects of electronegativity difference on the size of the bonded charge concentrations were reported. The effects were found to parallel the VSEPR argument that the bonded pair is more concentrated on the more electronegative atom; i.e., going from NH_3 to NF_3 the size of the bonded charge concentration on nitrogen *decreased*. Hence one would expect the bonded charge concentrations on tellurium in $TeCl_6^{2-}$ to be much smaller than the corresponding ones in XeF_6, for example. In addition to a reduction in the size of the bonded charge concentrations on the central atom, the increase in electronegativity difference would also result in a more closed-shell-like interaction. As this work suggests, such an increase in the closed-shell nature of the atomic interactions would lead to increased fluxionality. These predictions could be tested by an analysis of the calculated charge distributions of XeF_6 and $TeCl_6^{2-}$. Nevertheless this work suggests that any AX_6E system will show some, possibly very small, distortion from O_h symmetry *in the gas phase* arising from the presence of a nonbonded charge concentration on A.

Gimarc et al. have presented a qualitative MO argument to rationalize the observed symmetries of various AX_6E systems.[26] They argue that the larger the electronegativity difference between the central atom and the ligands, the less the distorted geometry will be stabilized by in-phase overlap of the ligand AO's comprising the totally symmetric HOMO. While this model makes the same predictions as above, it focuses on a single orbital. The atomic charges presented here suggest that the dominant ligand–ligand interaction (indirect since the fluorine atoms do not share an interatomic surface) is electrostatic repulsion, even when the electronegativity difference is minimized.

Connection between the SOJT Model and the Properties of the Charge Density

The SOJT model only requires knowledge of the symmetries of the lowest lying excited state (or unoccupied orbital) to make predictions of chemical interest. The energies of the virtual orbitals are largely determined by the distribution of charge in the occupied orbitals. Thus the SOJT model is inherently dependent on the ground-state charge distribution. In the previous section, although it was clear from just the properties of the charge distribution that ClF_6^- would be a very fluxional molecule, it was not clear *how* the molecule would most easily undergo this fluctuation. The SOJT model was used to determine the symmetry of this process. Perhaps information contained in the Laplacian distribution may provide a link between the static properties described by ρ_{00}, which can be determined experimentally, and the dynamical properties described by ρ_{0k}, which cannot. For instance in ClF_6^- there are three possible transition states that would lead to pseudorotation: C_{2v}, C_{4v}, and O_h. Along the lines of the VSEPR model the C_{2v} transition state minimizes the repulsive interactions between bonded and nonbonded charge concentrations that are less than 90° apart; hence, the easiest pathway for pseudorotation should be through a C_{2v} transition state, as is found.

Acknowledgment. I thank the Xerox Research Centre of Canada for the award of a Graduate Research Fellowship during 1984–1985.

Note Added in Proof. Within the framework of the present theory[14] one can partition the fluxional activation barrier into atomic contributions, $\Delta E(\Omega) = E(\Omega)_{trans} - E(\Omega)_{equil}$. $\Delta E(\Omega) > 0$ indicates the atom is less stable in the transition state, while $\Delta E(\Omega) < 0$ indicates the opposite. A similar partitioning of singlet–triplet energy gaps in carbenes has recently been reported.[18] With respect to the numbering scheme in Figure 4, the values for ClF_6^- are as follows (kcal/mol): $\Delta E(Cl) = -17$, $\Delta E(F1) = +44$, $\Delta E(F2(3)) = -8$, $\Delta E(F4) = -7$, $\Delta E(F5(6)) = -1$. The corresponding values for ClF_3 are as follows (kcal/mol): $\Delta E(Cl) = -26$, $\Delta E(F_{ax}) = +57$, $\Delta E(F_{eq}) = -42$. These numbers are to be compared with the data in Table II. Interestingly, the chlorine atom becomes *more* stable in the transition state for both systems. As should be expected, the destabilization in both systems is incurred by removing electrons from one or more fluorine atoms. It is instructive that it costs more energy to remove 0.03 e from the axial fluorine in ClF_3 (initially $q = -0.52$ e) than to remove 0.16 e from F1 in ClF_6^- (initially $q = -0.66$ e). While there are additional factors determining $\Delta E(\Omega)$, we feel that these data suggest that the fluxional behavior of these, and presumably other similar systems, strongly depends on the extent of "saturation" of the ligands.

Registry No. ClF_6^-, 42278-52-4.

(26) Gimarc, B. M.; Liebman, J. F.; Kohn, M. *J. Am. Chem. Soc.* **1978**, *100*, 2334.

Contribution from the Chemistry Department, University of British Columbia, Vancouver, BC, Canada V6T 1Y6

Mass Spectral Studies on the Thermal Decomposition of S_4N_4 and the Mechanism for Formation of $(SN)_x$

Elizabeth Besenyei,† Guenter K. Eigendorf, and David C. Frost*

Received March 25, 1986

A mechanism for the polymerization of $(SN)_x$ is proposed on the basis of a mass spectrometric study of the thermal decomposition of S_4N_4. The temperature dependence of the relative ion abundances and also the appearance potentials of the spectral fragments originating from S_4N_4 and S_2N_2 indicate that thermal decomposition produces these fragments as neutral species. We propose a fragmentation scheme in which reactions in the main pathway from S_4N_4 to SN are reversible and side reactions leading to loss of nitrogen and sulfur are not. In the presence of silver wool the transformation of S_2N_2 to $(SN)_2$ occurs, the latter being the starting material for the polymer. Both the thermal fragmentation of S_4N_4 to S_2N_2 and the transformation of S_2N_2 to $(SN)_2$ are facilitated by increasing the temperature, which also leads to the loss of nitrogen atoms. The polymerization process involves the reaction of $(SN)_2$ with SN originating from S_2N_2.

Introduction

Tetrasulfur tetranitride (S_4N_4) is the most well-known and characterized sulfur–nitrogen compound and provides the starting material for much chemistry in this area (see the reviews by Heal[1,2] and Labes et al.[3]).

Among the many diverse reactions of S_4N_4, thermal decomposition is of particular interest, since it leads to the synthesis of the unusual anisotropic three-dimensional metallic polymer $(SN)_x$.

* To whom correspondence should be addressed.
† Permanent address: Microelectronic Enterprise, 1044-Budapest, Hungary, Fôti U. 56.

(1) Heal, H. G. *Adv. Inorg. Chem. Radiochem.* **1972**, *15*, 375.
(2) Heal, H. G. *The Inorganic Heterocyclic Chemistry of Sulfur, Nitrogen and Phosphorus*; Academic: London, 1980; p 115.
(3) Labes, M. M.; Love, P.; Nichols, F. L. *Chem. Rev.* **1979**, *79*, 1.
(4) Mikulski, C. M.; Russo, P. J.; Saran, M. S.; MacDiarmid, A. G.; Garito, A. F.; Heeger, A. J. *J. Am. Chem. Soc.* **1975**, *97*, 6358.
(5) Cohen, M. J.; Garito, A. F.; Heeger, A. J.; MacDiarmid, A. G.; Mikulski, C. M.; Saran, M. S.; Kleppinger, J. *J. Am. Chem. Soc.* **1976**, *98*, 3844.

0020-1669/86/1325-4404$01.50/0